ACS Macro Letters

Letter

pubs.acs.org/macroletters

Enhanced Water Vapor Blocking in Transparent Hybrid Polymer–Nanocrystal Films

Eun Seon Cho,[†] Christopher M. Evans,[‡] Emily C. Davidson,[‡,§] Megan L. Hoarfrost,[§] Miguel A. Modestino,[§,∥] Rachel A. Segalman,[‡] and Jeffrey J. Urban*[,†]

[†]The Molecular Foundry, Materials Sciences Division, Lawrence Berkeley National Laboratory, Berkeley, California 94720, United States

[‡]Departments of Chemical Engineering and Materials, University of California, Santa Barbara, Santa Barbara, California 93106, United States

[§]Department of Chemical and Biomolecular Engineering, University of California, Berkeley, California 94720, United States

Supporting Information

ABSTRACT: Highly transparent and effective encapsulating materials have become increasingly important for photovoltaic (PV) modules to prevent water vapor molecules from permeating PV cells. The composite consists of block copolymer (PS-*b*-P2VP), comprised of hydrophobic and hydrophilic parts, and hygroscopic nanocrystals (Magnesium Oxide, MgO) incorporated to enhance water vapor blocking by both presenting obstacles for mass transport and also scavenging water molecules. The water vapor transmission rate (WVTR) values were reduced ~3000 times, compared to homopolymer (PS), for both polymer and composite samples. Achieving both high transparency and low WVTR, it is expected that the composite materials can function as an excellent water vapor blocking layer for PV modules.

Highly efficient gas barrier materials are required for a wide variety of applications, from food and drug packaging to electronic displays, devices, and photovoltaic cells.[1,2] In particular, thin, flexible, and transparent coatings with excellent oxygen and moisture barrier properties are critical in photovoltaic modules and electronic devices, to ensure reliability and improve their life span. Metal or inorganic films can function as superior oxygen and moisture barriers.[3] However, their fabrication involves an expensive manufacturing process, such as atomic layer deposition or chemical vapor deposition, which are not cost-effective and challenging for large-scale manufacture.[4] Moreover, requirements of flexibility, strong adhesion, and transparency strongly limit their use; hence, polymer-based materials are commonly used for gas barrier applications in functional devices.[5,6] Currently, many barrier coatings for photovoltaics have employed hydrophobic polymers like ethylene vinyl acetate (EVA); however, they provide merely adequate barrier properties. For new, upcoming technologies such as organic–inorganic perovskites great enhancements in barrier properties will be required.[7] In this work, we demonstrate a new approach to enhancing the gas barrier properties of materials. We develop a hybrid organic–inorganic composite material which relies on self-assembly of poly(styrene-*b*-2-vinylpyridine) (PS-*b*-P2VP) block copolymers with inorganic magnesium oxide (MgO) nanocrystals. This provides transport obstacles for incoming water molecules while also enabling moisture scavenging at the surfaces of the hygroscopic MgO crystals; we subsequently measure a 10^3 enhancement in performance over the homopolymer (PS).

For an effective gas barrier, it is necessary to reduce gas permeability itself, by selecting an intrinsically low-solubility material as a template of interest.[8,9] Barrier properties can be further improved by adding inorganic flakes into the films, which present mass transport obstacles, leading to an extended diffusion path and consequent lower diffusivity for permeating molecules.[10,11] Moreover, reactive groups can be incorporated into the barrier film, to capture diffusing molecules. For example, colloidal desiccants could be impregnated to scavenge water molecules.[12−14] These additives will need to be well-distributed in the film, as agglomeration of these particles deteriorates the gas barrier properties and increases light scattering drastically, decreasing light reaching the module.[15]

Here, we report a new approach to water vapor barrier composite materials—we have developed a superstructured composite material—composed of block copolymers and hygroscopic nanocrystals, with hierarchical order. We have designed this composite material to impede the ingress of water by multiple cooperative mechanisms at different length scales, which include solubility reduction, presenting obstacles to transport paths, and chemical reactivity (Figure 1(a)). This design also keeps the particles well dispersed and below the size at which light scattering would have a significant impact. Generally speaking, the field of polymer composites has been

Received: December 4, 2014
Accepted: December 9, 2014
Published: December 24, 2014

DOI: 10.1021/mz500765y
ACS Macro Lett. 2015, 4, 70−74

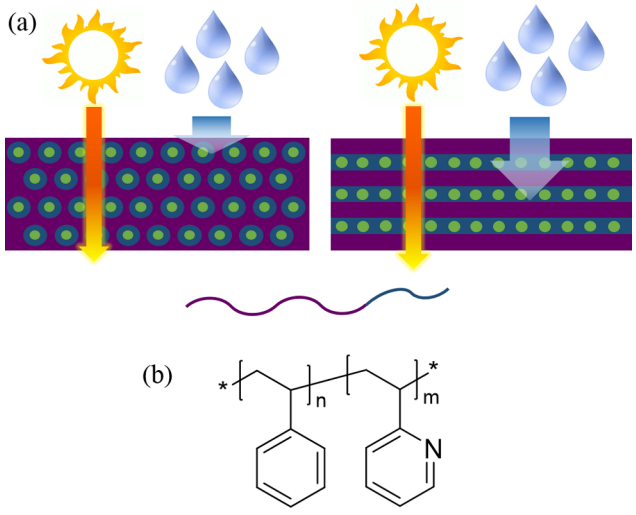

Figure 1. (a) Illustrations of PS-*b*-P2VP(S)-MgO (left) and PS-*b*-P2VP(L)-MgO (right) (PS (purple), P2VP (blue), MgO (green)) and (b) chemical structure of PS-*b*-P2VP.

fertile and touched many application areas, as incorporation of nanocrystals has been demonstrated to enhance material properties such as mechanical strength and electrical and magnetic characteristics.[16] However, even in many of these applications the microstructures are quite simple and do not take advantage of some of the unique self-assembly properties of block copolymers. Thus, there remain strong opportunities for polymer composites using block copolymers, as they can be made to self-assemble into unique structures on the nanometer scale, leading to complex 3D distributions of nanocrystals.[17,18] Here, we utilize the self-assembly characteristics of block copolymers to develop advanced water vapor barrier materials which incorporate hygroscopic nanocrystals in a well-defined structural arrangement. The hygroscopic nanocrystals, dispersed in the block copolymer matrix, and hydrophilic blocks provide obstacles to diffusion path for water molecules and at the same time act as reactive species, scavenging water molecules. Further, we test two different block copolymer morphologies to understand the role of polymer architecture on water vapor properties. Specifically, to examine the influence of block copolymer morphology on water transmission properties, two poly(styrene-*b*-2-vinylpyridine) (PS-*b*-P2VP) with both hydrophobic and hydrophilic blocks were used, referred to as PS-*b*-P2VP(S) and PS-*b*-P2VP(L), as shown in Figure 1(a) and (b). Here the S refers to a system which consists of poly(2-vinylpyridine) spheres in a PS matrix and L refers to a system consisting of alternating lamellae of poly(2-vinylpyridine) and polystyrene. The copolymers were synthesized via anionic polymerization as previously described.[19] The molecular weight of the PS block was determined via gel permeation chromatography (GPC), and the total molecular weight of the copolymer was determined using ^{1}H NMR (due to the tendency of the very polar P2VP block to adhere to the GPC columns, resulting in inaccurate molecular weight estimates for the block copolymer). The molecular weight of PS-*b*-P2VP(S) is 50 000 g/mol with f_{P2VP} (volume fraction of P2VP) = 0.16, and that of PS-*b*-P2VP(L) is 83 000 g/mol with f_{P2VP} = 0.40. For a hygroscopic nanocrystal, magnesium oxide (MgO) was chosen and prepared as previously reported.[20] The synthesized MgO (4 nm in diameter) was characterized via X-ray diffraction (XRD) and TEM (Figure S1, Supporting Information). One of the major obstacles to adding inorganic particulate into the polymer is a tendency of the nanocrystals to reduce the optical transparency of the film. Here, the nanometer scale and excellent dispersion in the P2VP domain allowed the films to remain transparent (Figure 2).

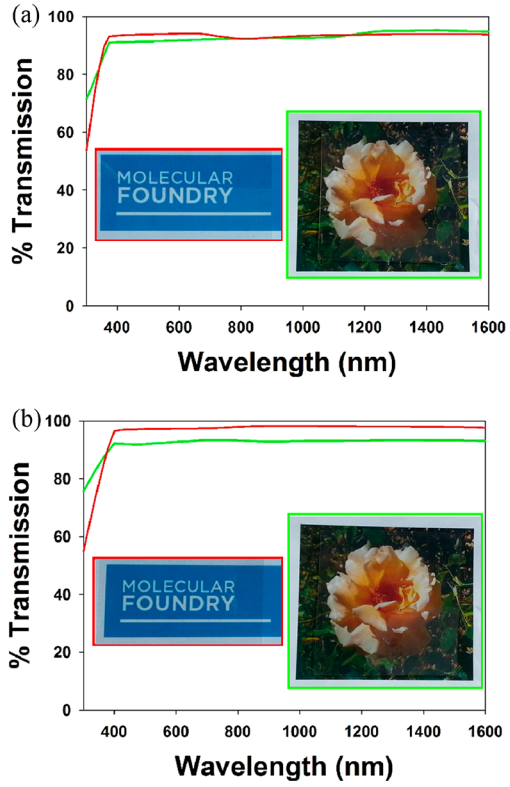

Figure 2. UV−vis spectra and pictures of (a) PS-*b*-P2VP(S) (red) and PS-*b*-P2VP(S)-MgO (green) and (b) PS-*b*-P2VP(L) (red) and PS-*b*-P2VP(L)-MgO (green) on PET substrate.

In this study, films were prepared from four material systems: PS-*b*-P2VP(S), PS-*b*-P2VP(S)-MgO, PS-*b*-P2VP(L), and PS-*b*-P2VP(L)-MgO. Two of these (PS-*b*-P2VP(S) and PS-*b*-P2VP(L)) are bare block copolymer films, and the other two (PS-*b*-P2VP(S)-MgO and PS-*b*-P2VP(L)-MgO) are the analogous block copolymer morphologies, but self-assembled with the MgO nanocrystals in the P2VP domains. With these films, the effects of block copolymer microstructure and water-scavenging capability of the nanocrystals were investigated. The composite of PS-*b*-P2VP and MgO was prepared by mixing them at concentrations of 3 and 0.5 wt %, respectively, in toluene. Each sample solution was coated onto a substrate, leading to a thin film. All samples were annealed at 150 °C (above the T_g of both blocks) for 3 days to allow the system to achieve an equilibrium structure. PS-*b*-P2VP(S) forms a spherical morphology; P2VP spheres are embedded in the PS matrix with well-ordered BCC structure; while PS-*b*-P2VP(L) has a lamellar structure, with lamellae stacked parallel to the substrate. This parallel orientation is a well-documented result which originates from the strong interaction between the poly(2-vinylpyridine) block and the substrate.[21] The schematic structures of each composite were illustrated in Figure 1(a), with the chemical structure of PS-*b*-P2VP shown in Figure 1(b). A high transparency (>92% transmittance in visible range, Figure 2) was achieved for all samples (both pure block

DOI: 10.1021/mz500765y
ACS Macro Lett. 2015, 4, 70−74

polymers and the block copolymer hybrids), as shown in Figure 2; this indicates that the MgO nanocrystals are well-distributed in the composite samples and not aggregating or undergoing macroscale phase segregation.

Morphological study of these composites was performed using X-ray scattering and mass spectrometry to elucidate the detailed microstructure of the composite films. Dynamic secondary ion mass spectrometry (d-SIMS) was also performed to further characterize the morphology of the composite (Figure 3) and provide information on the distribution of MgO nanocrystals throughout the films. In particular, we focused on the peaks from the mass 26, which originates from a mixture of C_2H_2 and CN and from the mass 24, coming from C_2 and mainly Mg. Considering the chemical structure, the mass 26 represents a characteristic distribution of P2VP, and the mass 24 indicates the presence of MgO. For both spherical and lamellar morphologies, the signals from the mass 26 oscillate due to the layered presence of the poly(2-vinylpyridine) by the BCC structure in PS-*b*-P2VP(S) and alternating lamellae for PS-*b*-P2VP(L).[22] The oscillation in the mass 24 signal in the composite is substantially larger than in the block copolymer sample, indicating that the Mg signal is mimicking the layered structure of the block copolymer nanostructure. Noticeably, the oscillations in the mass 26 and 24 peaks are in-phase in the composite samples, which supports the model of MgO nanocrystals existing in the P2VP domain. In the case of the lamellar system, the 24 signals are approximately 3 nm deeper than the 26 signals, implying that MgO nanocrystals prefer to be near the more polar CN groups but are located near the interface of PS and P2VP, rather inside P2VP lamella. From the d-SIMS depth profiles, it can be deduced that MgO nanocrystals are self-assembled into the poly(2-vinylpyridine) domain of the lamellar block copolymer morphology as well. Furthermore, the periodicity of the mass 26 signal from the composite is slightly larger than in the bare block copolymer by 2.71% and 7.67%, for PS-*b*-P2VP(L) and PS-*b*-P2VP(S), respectively. This is consistent with the expectation that the P2VP domain will undergo some swelling as a result of the presence of MgO. This feature is more prominent in the sphere-forming block copolymer, due to the smaller repeat distance of the nanostructure.

To examine the stability under high temperature and humidity of the samples, the morphologies of PS-*b*-P2VP(S) and its composite (PS-*b*-P2VP(S)-MgO) were also investigated via small-angle X-ray scattering (SAXS) and are displayed in Figure 4 as radially averaged 1-D plots (more SAXS data including 2-dimensional patterns are in Supporting Information.).[23] PS-*b*-P2VP(S) shows clear BCC structure sphere morphology, both with and without incorporation of nanocrystals. The primary peak shift as a consequence of incorporating MgO nanocrystals into the polymer was not observed due to a relatively higher density of MgO than that of the polymer, leading to even smaller volumetric perturbation in SAXS. Furthermore, SAXS measurements were performed after exposure of the films to 100% humidity and 80 °C for 3 days, to examine the stability against heat and moisture. These measurements, shown in Figure 4, show no significant changes in peak positions for either of the PS-*b*-P2VP(S) samples. This indicates that there was no noticeable water absorption for both cases since the domain swelling and subsequent peak shifts and profiles would be anticipated if water intake were significant. Further, this implies that P2VP spheres embedded in a PS matrix provide significant transport limitations for water to permeate into them. We also note that there are no peaks or distortions arising from the agglomeration of particles indicating that they remain well-dispersed in the domains. Furthermore, the domain size of PS-*b*-P2VP(S) and PS-*b*-

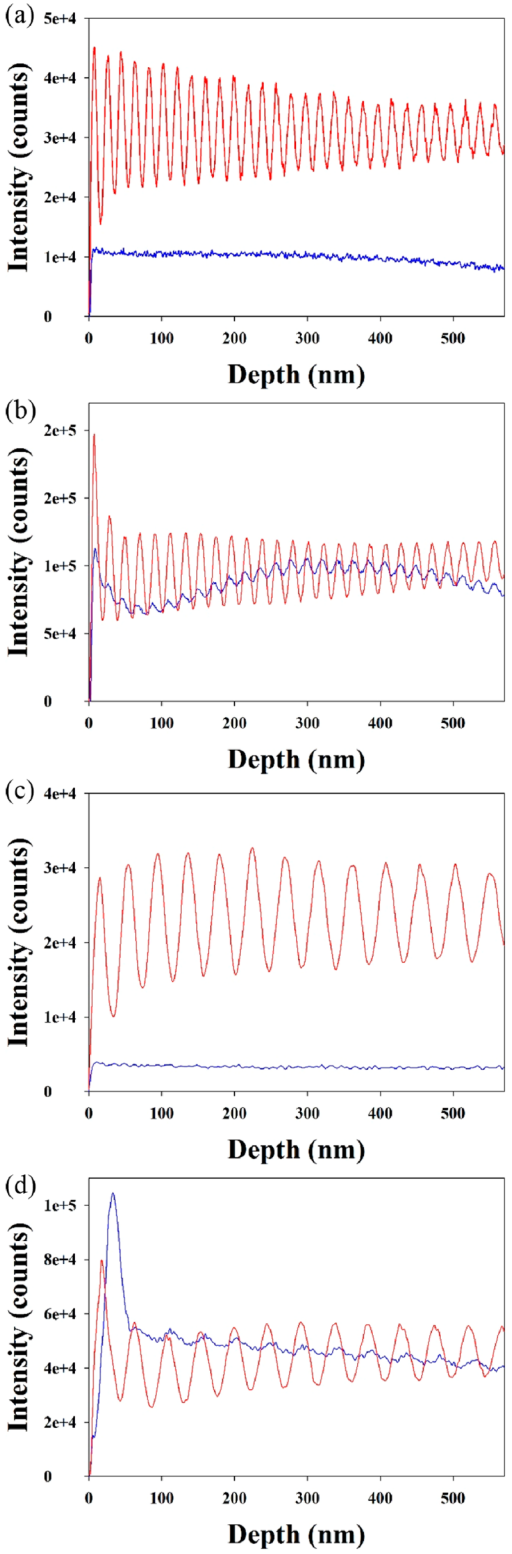

Figure 3. SIMS depth profiles of (a) PS-*b*-P2VP(S), (b) PS-*b*-P2VP(S)-MgO, (c) PS-*b*-P2VP(L), and (d) PS-*b*-P2VP(L)-MgO. Red and blue lines correspond to the peaks from the mass 26 and 24, respectively.

DOI: 10.1021/mz500765y
ACS Macro Lett. 2015, 4, 70−74

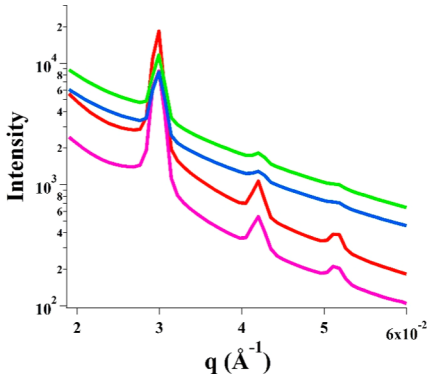

Figure 4. SAXS patterns of PS-*b*-P2VP(S) and PS-*b*-P2VP(S)-MgO. Red and green lines represent each PS-*b*-P2VP(S) and PS-*b*-P2VP(S)-MgO, respectively, before exposure to 80 °C and 100% humidity. Pink and blue lines correspond to each PS-*b*-P2VP(S) and PS-*b*-P2VP(S)-MgO, respectively, after exposure to 80 °C and 100% humidity for 3 days.

P2VP(S)-MgO is 21 nm for both structures based on analysis of the SAXS data. Importantly, these sizes closely match the values calculated from the SIMS data, which are 19.7 and 21.1 nm for PS-*b*-P2VP(S) and PS-*b*-P2VP(S)-MgO, respectively.

Water vapor transmission rate (WVTR) measurements were performed to quantify the specific water vapor blocking characteristics of our materials, and all measurements were compared to a standard value of approximately 15.5 g mil/(m^2 day) for a conventional EVA sample at 38 °C and 100% relative humidity. The WVTR values of both polymer and composite samples were measured at 40 °C and at a relative humidity of 100% at Mocon Inc., USA, with the results summarized in Table 1. In order to reliably compare the different composite

Table 1. WVTR Values of the Samples at 38 °C and at a Relative Humidity of 100%[a]

	thickness (nm)	WVTR g mil/(m^2 day)
PS-*b*-P2VP(S)	523 ± 13	3.076×10^{-3}
PS-*b*-P2VP(S)-MgO	370 ± 10	2.118×10^{-3}
PS-*b*-P2VP(L)	517 ± 1	3.285×10^{-3}
PS-*b*-P2VP(L)-MgO	460 ± 10	2.845×10^{-3}
PS[b]		7.286

[a]All values were normalized to 1 mm thick films. [b]WVTR of PS is from the literature measured at 40 °C and 90% relative humidity.

block copolymer films, the WVTR values were normalized to 1 mm thick films. The WVTR values of the block copolymer composite films are greatly reduced in comparison to the pure PS homopolymer (WVTR = 7.286 g mil/(m^2 day) at 40 °C and 90% relative humidity).[24] This reduction, noticeable for all block copolymer samples, is attributed to the self-assembly of the block copolymer into complex morphologies, for example, the spherical and lamellar nanostructures in which hydrophilic spheres or lamella are distributed among hydrophobic layers, respectively. Furthermore, irrespective of morphology, the WVTRs for all samples containing MgO nanoparticles are reduced in comparison to the same samples without nanoparticles. This result is consistent with the nanoparticles in the hydrophilic blocks acting as water molecule scavengers, due to their reactive, oxygen-rich surfaces. Comparing morphologies, we observe that spherical morphologies exhibit slightly better water vapor blocking ability than the lamellar morphologies (across similar samples, i.e., block copolymer only vs block copolymer with nanocrystals). Interestingly, barrier properties were enhanced across all samples via incorporation of hygroscopic nanocrystals into the polymer, despite the fact that this required introduction of a hydrophilic domain into the system to stabilize them. Strikingly, with the addition of only 0.5 wt % of nanocrystals in these samples, water-blocking ability was improved by as much as 30%. Higher densities of nanocrystals were not pursued at this time as incorporation of these into active PV modules requires high optical transparency. Furthermore, due to the hygroscopic characteristics of the nanocrystals, this barrier layer would not be saturated during long-term operation, since absorbed water molecules would be emitted under elevated temperature and low humidity, which is an ordinary operating condition for PV modules.

In summary, the development of new encapsulating materials for both established absorber layers and new technologies are required because they are environmentally sensitive to degradation from water and other molecular species. Current encapsulating materials, however, have been selected primarily on the basis of cost-effectiveness and do not perform well in comparison to physical limits, thus putting photovoltaic modules at risk over time. We successfully fabricated composites of block copolymer (PS-*b*-P2VP) and hygroscopic nanocrystals (MgO) for the purpose of enhancing the water vapor barrier behavior of encapsulants. The composite was designed to enhance water vapor blocking effectively via two mechanisms: presenting obstacles to transport paths and scavenging water molecules via both hydrophilic blocks and hygroscopic nanocrystals. The effects of block copolymer morphology were also examined, by comparing spherical and lamellar structures. It was shown that the lamellar structure is more susceptible to water vapor, while both types of block copolymer structures greatly contribute to an effective water vapor blocking, compared to homopolymers. Also, the incorporation of nanocrystals was able to reduce WVTR by 30%, even for only 0.5 wt % of nanocrystal loading. This work provides a platform for designing new classes of hybrid encapsulant materials to aid in the protection of new, sensitive photovoltaic technologies.

■ ASSOCIATED CONTENT

Supporting Information

Experimental details and additional data. This material is available free of charge via the Internet at http://pubs.acs.org

■ AUTHOR INFORMATION

Corresponding Author

*E-mail: jjurban@lbl.gov.

Present Address

[‖]Optics Laboratory, Ecole Polytechnique Fédérale de Lausanne (EPFL), 1015, Switzerland.

Notes

This report was prepared as an account of work sponsored by an agency of the United States Government. Neither the United States Government nor any agency thereof, nor any of their employees, makes any warranty, express or implied, or assumes any legal liability or responsibility for the accuracy, completeness, or usefulness of any information, apparatus, product, or process disclosed, or represents that its use would not infringe privately owned rights. Reference herein to any

DOI: 10.1021/mz500765y
ACS Macro Lett. 2015, 4, 70−74

specific commercial product, process, or service by trade name, trademark, manufacturer, or otherwise does not necessarily constitute or imply its endorsement, recommendation, or favoring by the United States Government or any agency thereof. The views and opinions of authors expressed herein do not necessarily state or reflect those of the United States Government or any agency hereof.
The authors declare no competing financial interest.

■ ACKNOWLEDGMENTS

This material is based upon work supported by the Department of Energy (DOE) through the Bay Area Photovoltaic Consortium (BAPVC) under Award Number DE-EE0004946 and also in part under the US-India Partnership to Advance Clean Energy-Research (PACE-R) for the Solar Energy Research Institute for India and the United States (SERIIUS), funded jointly by the U.S. Department of Energy (Office of Science, Office of Basic Energy Sciences, and Energy Efficiency and Renewable Energy, Solar Energy Technology Program, under Subcontract DE-AC36-08GO28308 to the National Renewable Energy Laboratory, Golden, Colorado) and the Government of India, through the Department of Science and Technology under Subcontract IUSSTF/JCERDC-SERIIUS/2012 dated 22nd Nov. 2012. Work at the Molecular Foundry was supported by the Office of Science, Office of Basic Energy Sciences, of the U.S. Department of Energy under Contract No. DE-AC02-05CH11231. J.J.U. and R.A.S. conceived of and designed the experiments. E.S.C. performed the materials integration and characterization, supported by Department of Energy Grant no. DE-FG07ER46426, by the Bay Area Photovoltaic Consortium (BAPVC), funded under the Sunshot Initiative of DOE. E.S.C. performed WVTR work using support from the Joint India-US research consortium funded under the Joint Clean Energy Research and Development Center (JCERDC) supported by DOE. E.C.D. and M.L.H were funded by NSF grant no. NSF-DMR-1206296. Polymers were provided by C.M.E. and M.L.H., and SAXS measurements were performed by E.C.D. and M.A.M, supported by the Joint Center for Artificial Photosynthesis (JCAP), a DOE Energy Innovation Hub, supported through the Office of Science of the U.S. Department of Energy under Award Number DE-SC0004993. Work at the Molecular Foundry was supported by the Office of Science, Office of Basic Energy Sciences, at the U.S. Department of Energy (DOE). SAXS measurements were performed at beamline 7.3.3 of the Advanced Light Source (ALS) at Lawrence Berkeley National Laboratory (LBNL) and at beamline 1-5 at Stanford Synchrotron Radiation Laboratory (SSRL). The authors are grateful to Dr. Chris Tassone at SSRL. Also, the authors sincerely appreciate Dr. Tom Mates for assisting SIMS and discussing data analysis and Dr. Jason Forster for ellipsometer. The authors greatly thank Dupont Teijin Films for providing the PET substrate.

■ REFERENCES

(1) Lange, J.; Wyser, Y. *Packag. Technol. Sci.* **2003**, *16*, 149−158.
(2) Choi, M. C.; Kim, Y.; Ha, C. S. *Prog. Polym. Sci.* **2008**, *33*, 581−630.
(3) Kim, N. R.; Lee, Y. D.; Paek, K. K.; Lee, J. W.; Kim, J. K.; Hwang, S. W.; Ju, B. K. *Surf. Interface Anal.* **2007**, *39*, 64−68.
(4) Barker, C. P.; Kochem, K. H.; Revell, K. M.; Kelly, R. S. A.; Badyal, J. P. S. *Thin Solid Films* **1995**, *259*, 46−52.
(5) Yang, Y. H.; Haile, M.; Park, Y. T.; Malek, F. A.; Grunlan, J. C. *Macromolecules* **2011**, *44*, 1450−1459.
(6) Koros, W. J. *ACS Symp. Ser.* **1990**, *423*, 1−21.
(7) Green, M. A.; Ho-Baillie, A.; Snaith, H. J. *Nat. Photonics* **2014**, *8*, 506−514.
(8) Comyn, J. *Polymer permeability*; Elsevier Applied Science Publishers: London; New York, 1985; p viii, 383 p.
(9) Koros, W. J. Polymer Chemistry Inc.; *Meeting, Barrier polymers and structures*; American Chemical Society: Washington, DC, 1990; p 406.
(10) Seethamraju, S.; Ramamurthy, P. C.; Madras, G. *RSC Adv.* **2013**, *3*, 12831−12838.
(11) Kunz, D. A.; Schmid, J.; Feicht, P.; Erath, J.; Fery, A.; Breut, J. *ACS Nano* **2013**, *7*, 4275−4280.
(12) Moggridge, G. D.; Lape, N. K.; Yang, C. F.; Cussler, E. L. *Prog. Org. Coat.* **2003**, *46*, 231−240.
(13) Solovyov, S. E. *J. Phys. Chem. B* **2006**, *110*, 17977−17986.
(14) Yang, C. F.; Nuxoll, E. E.; Cussler, E. L. *AIChE J.* **2001**, *47*, 295−302.
(15) Garcia, M. G.; Marchese, J.; Ochoa, N. A. *J. Appl. Polym. Sci.* **2010**, *118*, 2417−2424.
(16) Balazs, A. C.; Emrick, T.; Russell, T. P. *Science* **2006**, *314*, 1107−1110.
(17) Chiu, J. J.; Kim, B. J.; Kramer, E. J.; Pine, D. J. *J. Am. Chem. Soc.* **2005**, *127*, 5036−5037.
(18) Lin, Y.; Boker, A.; He, J. B.; Sill, K.; Xiang, H. Q.; Abetz, C.; Li, X. F.; Wang, J.; Emrick, T.; Long, S.; Wang, Q.; Balazs, A.; Russell, T. P. *Nature* **2005**, *434*, 55−59.
(19) Yokoyama, H.; Mates, T. E.; Kramer, E. J. *Macromolecules* **2000**, *33*, 1888−1898.
(20) Moon, H. R.; Urban, J. J.; Milliron, D. J. *Angew. Chem., Int. Ed.* **2009**, *48*, 6278−6281.
(21) CalistriYeh, M.; Park, E. J.; Kramer, E. J.; Smith, J. W.; Sharma, R. *J. Mater. Sci.* **1995**, *30*, 5953−5959.
(22) Yokoyama, H.; Kramer, E. J.; Hajduk, D. A.; Bates, F. S. *Macromolecules* **1999**, *32*, 3353−3359.
(23) Ilavsky, J. *J. Appl. Crystallogr.* **2012**, *45*, 324−328.
(24) Delassus, P. T. *Tappi J.* **1988**, *71*, 216−219.

DOI: 10.1021/mz500765y
ACS Macro Lett. 2015, 4, 70−74